Lawrence Berkeley National Laboratory

Title
Continuous time random walk analysis of solute transport in fractured porous media

Permalink
https://escholarship.org/uc/item/4x92159z

Author
Cortis, Andrea

Publication Date
2008-07-14

Peer reviewed

Continuous Time Random Walk Analysis of Solute Transport in Fractured Porous Media

Andrea Cortis and Jens Birkholzer

Lawrence Berkeley National Laboratory

Abstract

The objective of this work is to discuss solute transport phenomena in fractured porous media, where the macroscopic transport of contaminants in the highly permeable inter-connected fractures can be strongly affected by solute exchange with the porous rock matrix. We are interested in a wide range of rock types, with matrix hydraulic conductivities varying from almost impermeable (e.g., granites) to somewhat permeable (e.g., porous sandstones). In the first case, molecular diffusion is the only transport process causing the transfer of contaminants between the fractures and the matrix blocks. In the second case, additional solute transfer occurs as a result of a combination of advective and dispersive transport mechanisms, with considerable impact on the macroscopic transport behavior. We start our study by conducting numerical tracer experiments employing a discrete (microscopic) representation of fractures and matrix. Using the discrete simulations as a surrogate for the "correct" transport behavior, we then evaluate the accuracy of macroscopic (continuum) approaches in comparison with the discrete results. However, instead of using dual-continuum models, which are quite often

24   used to account for this type of heterogeneity, we develop a macroscopic model based on

25   the Continuous Time Random Walk (CTRW) framework, which characterizes the

26   interaction between the fractured and porous rock domains by using a probability

27   distribution function of residence times. A parametric study of how CTRW parameters

28   evolve is presented, describing transport as a function of the hydraulic conductivity ratio

29   between fractured and porous domains.

30

31   **Introduction**

32

33   The internal heterogeneity of fractured porous formations is a significant obstacle to the

34   prediction of solute transport processes (Berkowitz, 2002). The macroscopic transport of

35   contaminants in such systems is mainly carried out in high-permeable, interconnected

36   fractures, but most of the capacity for storing a pollutant is provided by the low-

37   permeability porous matrix. Because of the much slower transport in the matrix, steep

38   concentration gradients may occur between the fractures and the porous blocks, giving

39   rise to a local disequilibrium. The terms "macroscopic" and "local" or "microscopic" are

40   used in this paper to define different scales of interest. The macroscopic scale

41   incorporates a large number of individual fractures and matrix blocks, e.g., between a

42   contaminant source and a monitoring well. In contrast, the local (microscopic) scale is on

43   the order of single fractures and single matrix blocks. The local disequilibrium situation

44   with regard to the solute concentrations in fractures and matrix can lead to significant

45   solute transfer at the fracture/matrix interfaces. This local transfer can strongly influence

46   the macroscopic solute transport in a fractured porous formation, and thus needs to be

47   accounted for in numerical models (Berkowitz, 2002).

48

Generally, the numerical simulation of flow and transport processes in fractured porous media can be performed with discrete models or continuum models (e.g., Berkowitz, 2002; Neuman, 2005). Discrete models describe the spatial structure of the fracture-matrix system in great detail on a microscopic level, and thus allow for a more accurate simulation than continuum models. However, since discrete models are limited in their applicability to field problems, upscaling methods are commonly employed to develop macroscopic models, simulating the flow and solute transport behavior in sufficiently large computational cells and assigning suitably averaged "effective" properties to them. In fractured porous formations, where the local disequilibrium between fractures and matrix cannot be neglected, researchers have often applied so-called dual-continuum models (Barenblatt et al., 1960). Here, the heterogeneous formation is separated into two superimposed, interacting media, one representing the fracture system with high conductivity, the other representing the porous rock matrix with high storage capacity. Because both media are treated as different systems, the flow and transport processes are described by two separate sets of equations coupled by transfer terms to account for the exchange of mass at the common boundary.

Despite the simplification with regard to neglecting microscopic transport processes, numerical modeling of dual-continuum systems is still a complicated process. For example, different types of dual-continuum approaches are needed depending on the hydrologic characteristics of the porous matrix. In the general form of a dual-continuum model, the regional flow and transport processes take place in both domains. In many

71 formations, however, the regional flow and transport processes in the matrix continuum

72 can be neglected because the hydraulic conductivity of the matrix is almost negligible

73 compared to that of the fracture continuum, such as in crystalline rocks or shale (Bodin et

74 al., 2003). In such cases, the matrix continuum acts as a local storage domain for the

75 regional flow and transport in the fracture continuum. The governing equation for the

76 matrix continuum can then be simplified by eliminating the macroscopic flow and

77 transport terms so that only the local fluid flow or solute exchange with the fracture

78 continuum needs to be considered. In the first general form of a dual-continuum model,

79 we use the term "dual-permeability" (or mobile-mobile) model; the latter case is referred

80 to as a "dual-porosity" (or mobile-immobile) model (Simunek et al., 2003). Note that in a

81 dual-porosity model, the local fluid flow between fracture and matrix continua may be

82 neglected, e.g., when the flow field is steady-state as assumed in this paper (i.e., no local

83 pressure gradient between fractures and matrix) or when the matrix permeability is

84 sufficiently small. Matrix diffusion is then the only relevant solute transfer process at the

85 fracture-matrix interfaces.

86

87 A variety of dual-porosity (mobile-immobile) approaches have been described in the

88 literature, most of which with a focus on solute transport in fractured porous media.

89 Respective models have been developed with simple first-order transfer terms (e.g.,

90 Huyakorn et al., 1983a; Birkholzer and Rouve, 1994) or more complex higher-order

91 approaches, where local-scale detailed descriptions of diffusive transport are employed in

92 the immobile domain (e.g., Bibby, 1981; Huyakorn, 1983b, 1983c; Dykhuizen, 1990;

93 Zimmerman et al., 1990, 1993; Birkholzer and Rouve, 1994). Note that variations of

94   dual-porosity approaches have also been used to study solute-transport problems in

95   heterogeneous porous media bimodal permeability structures (e.g., Roth and Jury, 1993;

96   Haggerty and Gorelick, 1995; Feeley et al., 2000; Flach et al., 2004).

97

98   Macroscopic modeling of solute transport in dual-permeability (mobile-mobile) systems

99   is conceptually more challenging than in dual-porosity (mobile-immobile) systems. First,

100   the macroscopic transport processes need to be solved for in both continua, which

101   requires determination of hydrologic properties separately for the fractured and the

102   porous domain (e.g., Teutsch, 1988; Gerke and van Genuchten, 1993a). Furthermore, the

103   solute-transfer term needs to take into account not only diffusive transport, but also the

104   additional effects of advection and dispersion. Figure 1 schematically illustrates the

105   advective mass exchange between fractures and porous matrix, as solutes migrate within

106   matrix pores (driven by a regional gradient) and encounter flow in transverse fractures.

107   Birkholzer and Rouve (1994) proposed a dual-permeability approach with a specific

108   solute transfer term for such advective-dispersive mixing processes. In this approach, a

109   first-order exchange term is determined, based on the macroscopic flow in the matrix

110   continuum and the geometric characteristics of the fracture network. For dual-

111   permeability modeling of heterogeneous soils with high- and low-permeability regions,

112   Ahmadi et al. (1998), Cherblanc et al. (2003), and Cherblanc et al. (2007) developed a

113   volume averaging technique that allows definition of first-order transfer terms for

114   diffusive, dispersive, and advective processes.

115

116   As is apparent from the above discussion, dual-continuum models of various types are

117   available for simulating solute transport in fractured porous media. However, while dual-

118   porosity models have quite often been applied to field problems, dual-permeability

119   applications have been less frequent. One of the crucial problems encountered when

120   using dual-permeability models is the determination of the large-scale effective properties,

121   which include the macroscopic flow and transport properties of the two domains, as well

122   as the properties determining solute transfer between the two domains. This is not a

123   trivial task. For example, while *a priori* estimates of solute transfer coefficients have

124   been proposed for idealized subsurface geometries (e.g., Dykhuizen, 1990; Zimmerman

125   et al., 1990, 1993; Gerke and van Genuchten, 1993b; Gwo et al., 1998 [for diffusive

126   matrix transport]; Birkholzer and Rouve, 1994 [for advective matrix transport]), they are

127   generally derived from calibration to field measurements. Furthermore, the *a priori*

128   decision about the appropriate model to be used in a specific field situation—dual-

129   porosity or dual-permeability—can be difficult, depending on the time and length scale of

130   interest as well as the domain properties.

131

132   In this paper, we evaluate the applicability of the Continuous Time Random Walk

133   (CTRW) theory for modeling solute transport in fractured porous formations, as an

134   alternative to the traditional dual-continuum approach. The CTRW theory has been

135   developed to explain and model anomalous, i.e., non-Fickian, transport in heterogeneous

136   physical systems (Scher and Lax, 1973). Any deviation from perfect homogeneity

137   induces retardation and/or acceleration of the solute, which cannot be represented by

138   models based on the classical hypothesis of homogeneous transport. CTRW is an

139   effective upscaled method that treats unresolved (small-scale) heterogeneities

140   stochastically and resolved (large-scale) heterogeneities deterministically. CTRW has

141   found many useful applications in hydrogeological problems, including transport of

142   tracers in porous media (Bijecjic and Blunt, 2006), fracture networks (Berkowitz and

143   Scher, 1995, Noetinger et al., 2001a,b, Landereau et al., 2001), sandstones, sand columns,

144   unsaturated soils (Cortis and Berkowitz, 2004), karstic systems (Anwar et al., 2007), the

145   hyporheic zone (Boano et al., 2007), transient flow in highly heterogeneous permeable

146   systems (Cortis and Knudby, 2006), flow of emulsions in porous media (Cortis and

147   Ghezzehei, 2007), heat transfer in porous media (Emmanuel and Berkowitz, 2006), and

148   transport of biocolloids (Cortis et al., 2006).

149

150   Dentz and Berkowitz (2003) demonstrated that the CTRW method is formally equivalent

151   to the linear multirate mass-transfer (MRMT) concept (e.g., Haggerty and Gorelick,

152   1995). The dual-porosity approach is essentially a MRMT model with a specific mass-

153   transfer model accounting for heterogeneity in the solute exchange between mobile and

154   immobile regions. Our study aims at demonstrating that the CTRW framework not only

155   can substitute for dual-continuum approaches, but is generally applicable to fractured

156   porous formations over a wide range of matrix permeabilities. We do this by first

157   conducting numerical tracer experiments in discrete fracture-matrix systems (Berkowitz

158   et al., 1988, Birkholzer et al. 1993a,b, Birkholzer and Rouve, 1994, Rubin et al., 1996).

159   These simulations are assumed to represent the "correct" system behavior. In a second

160   step, the results of the discrete simulations are compared with the results from a

161   nonparametric best-fit solution of the CTRW method (Cortis, 2007).

2 Discrete Numerical Experiments

2.1 Methodology

Numerical tracer experiments are conducted using a discrete representation of individual fractures and matrix blocks, respectively. Because the flow and transport processes are simulated in great detail on a microscopic ("local") scale, we may assume that the discrete simulation results faithfully represent the transport corresponding to a given set of hydrologic properties, so that the results obtained using the CTRW method can be compared to these "correct" results.

Since our main interest here is phenomena related to fracture/matrix interaction and their impact on macroscopic solute transport, it is reasonable to restrict the discrete simulations to fractured formations with regular geometry and uniform properties. The randomness and heterogeneity of natural fracture networks would (1) create difficulties in interpreting the simulation results with regard to the purpose of our study, and (2) involve the difficult task of assigning effective continuum parameters. Issues of computational efficiency are to be considered as well, since the discrete simulation results need to be compared to continuum results on a sufficiently large scale.

Figure 2 illustrates the setup for the numerical experiments. An idealized formation is considered, with two orthogonal sets of parallel equidistant fractures embedded in porous permeable matrix blocks (Berkowitz et al., 1988; Birkholzer and Rouve, 1994; Lagendijk, 2005). A constant (steady-state) hydraulic gradient of 0.01 in the positive x-direction is imposed by prescribing appropriate hydraulic head boundary conditions at the inflow and

185 outflow cross sections of the model area. On the local scale, flow in the matrix follows

186 the direction of the gradient, whereas flow in the fractures follows the fracture axis. On

187 the macroscopic scale, however, both types of flow follow the positive x-direction, owing

188 to the symmetry of the fracture network. We simulate the migration of an ideal tracer

189 disposed uniformly along the inflow cross section, given by a relative concentration value

190 of one imposed at the inflow boundary of the model area. The solute migrates through the

191 model area in both the fractures and the porous permeable blocks; however, the transport

192 in the fractures is several orders of magnitude faster. Initially, the model area is not

193 contaminated.

194

195 Although the conceptual setup is highly idealized, it is consistent with the requirements

196 needed for the present study. First, it represents the tortuous flow paths through a natural

197 fracture network, providing a large interface for mixing between the fractures and the

198 porous blocks. Second, the flow and transport processes in the domain are symmetrical to

199 the x-axis, without any transverse dispersion stemming from the randomness and

200 heterogeneity of the fracture network. It is therefore possible to use the system's

201 symmetry and simulate only the long, thin sub domain depicted in the bottom of Figure 2,

202 with the upper and lower boundaries representing no-flow boundaries. As indicated in the

203 figure, the term "sector" refers to part of the model domain extending between two

204 adjacent fracture intersections. We consider model domains consisting of a hundred, 0.5

205 m long, sectors, so that the total length of the model domain is 50 m in the x–direction,

206 and 0.5 m in the y–direction.

207   The discrete simulation runs were performed with the standard GALERKIN-Finite-

208   Element-Code STRAFE6 using a Crank-Nicholson time weighting scheme (Lagendijk,

209   2005). Due to the heterogeneity of the formation, a refined discretization in space and

210   time was needed to meet the Peclet and Courant criteria. Triangle elements were used for

211   the porous matrix and one-dimensional line-elements for the fracture representation (see

212   example for two sectors in Figure 2, bottom). A total number of with 1,000 line elements

213   and 20,000 triangles was utilized, and simulation runs comprised up to 30,000 time steps.

214

215   Tables 1 and 2 summarize the geometrical and hydrological properties chosen for the

216   discrete simulations. These properties are similar to those used in the discrete numerical

217   experiments described in Birkholzer and Rouve (1994) and Lagendijk (2005). The

218   majority of them are kept constant in our study (Table 1), except for the hydraulic

219   conductivity in the matrix, which is varied in four sensitivity cases (Table 2). We expect

220   matrix conductivity to be the most important parameter defining (1) whether the fractured

221   porous formation is a mobile-immobile or a mobile-mobile system, and (2) whether the

222   solute exchange between fractures and matrix is dominated by diffusive or advective

223   processes. All values chosen represent reasonable parameters mentioned in the literature

224   as typical for actual field situations. Notice that the relevant fracture properties in Table 1

225   are given for single fractures, as represented in the discrete modeling exercise, but have

226   also been converted into fracture continuum parameters, as required in macroscopic

227   continuum approaches (fracture continuum conductivity and fracture continuum porosity).

228

229   Table 2 discusses the basic features of the four sensitivity cases. In Case 1, we consider a

230   small hydraulic conductivity in the matrix of 8.3×10^{-6} m/d; i.e., the porous matrix is

231   essentially impermeable. Cases 2 and 3 denote intermediate cases with conductivities of

232   2.0×10^{-3} m/d and 8.3×10^{-3} m/d, respectively, while Case 4 features a relatively high

233   matrix conductivity of 9.94×10^{-2} m/d. Notice the strong internal heterogeneity reflected

234   in the ratios of fracture to matrix continuum conductivity and transport velocity. With

235   respect to conductivity, these ratios range from 12,000 (Case 1) to 1 (Case 4); i.e., in the

236   latter case, the same magnitude of flow occurs in the two continua. With respect to

237   transport velocity, these ratios range from almost infinite (Case 1) to 250 (Case 4); i.e., in

238   all cases, the transport velocity in single fractures is much higher than the transport

239   velocity in the matrix. As discussed in Birkholzer and Rouve (1994), the internal

240   heterogeneity causes a solute-transport behavior in which the fast flow and transport in

241   the fractures is affected by more or less intense solute exchange with the matrix. In the

242   first case, with near-zero matrix permeability, molecular diffusion is the only transport

243   process causing the transfer of solutes between the fractures and the matrix blocks. In the

244   other cases, with increasing matrix conductivity, more and more solute mixing occurs

245   between fractures and the matrix, as a result of advective flow in the matrix, which has a

246   sizable impact on overall transport behavior (see Section 2.2).

247

248   **2.2   Simulation Results**

249   We shall first discuss simulation results on a local scale—i.e., on the scale of single

250   fractures and matrix blocks—to evaluate the basic phenomena of solute transport in

251   fracture-matrix systems. In Figure 3, we present the solute isoconcentration contours for

252   the discrete matrix blocks located in Sectors 3 and 4 of the model area. These sectors are

253   close enough to the contaminant source to feature a fast response, and yet far enough

254   away from it to be essentially unaffected by the inlet boundary condition. We then

255   discuss the macroscopic transport in the discrete fracture-matrix systems using

256   breakthrough curves (BTC, see Figure 4) obtained at selected locations along the model

257   domain (i.e., at 1 m, 5 m, 15 m, and 45 m from the inflow boundary, which corresponds

258   to 2, 10, 30, and 90 model sectors). The BTCs at these locations will be used to evaluate

259   the performance of the CTRW method.

260

261   Figure 3(a) depicts the discrete simulation results in Sectors 3 and 4 for Case 1, which

262   has an almost impermeable porous matrix. We notice a strong contaminant buildup near

263   the fractures, demonstrating that solutes migrate very fast in the fracture network. During

264   this fast advective transport, a small fraction of the solute migrates from the fractures into

265   the porous matrix. This process is slow: at 100 days, the major fraction of the matrix

266   blocks is not yet contaminated. The BTCs for Case 1 in Figure 4(a) exhibit the typical

267   transport behavior of dual-porosity (mobile-immobile) media. The tracer breakthrough

268   values initially increase very quickly, because of the large velocities in the fracture

269   network. The smaller the distance between observation point and tracer inlet, the more

270   significant the initial concentration buildup. Long tailing is observed after the initial

271   buildup, a result of the slow diffusive transfer between the fractures and the matrix pore

272   system. The dashed BTC indicates the local concentration differences between fractures

273   and matrix for a migration distance of 30 sectors. It is obvious that the formation would

274 need a very long time to equilibrate: significant local concentration differences can still

275 be observed at 3,000 days.

276

277 Concentration contours for Cases 2 and 3 are presented in Figures 3(b) and 3(c),

278 respectively, after 100 days of solute disposal. While the transport velocity in the

279 fractures is still orders of magnitude higher than in the matrix (Table 2), the impact of

280 increasing matrix permeability shows in the microscopic transport behavior. The

281 asymmetrical concentration contours are a result of advective-dispersive transport in the

282 matrix, acting in the positive x–direction. The diffusive transfer from the fractures into

283 the matrix is complemented by this advective-dispersive component—thus, the faster

284 concentration buildup in the matrix compared to Case 1. The effect of enhanced mixing

285 between fractures and matrix also shows in the BTCs in Figures 4(b) and 4(c), where,

286 compared to Case 1, equilibrium conditions are reached earlier and less tailing can be

287 observed.

288

289 Case 4 presented in Figures 3(d) and 4(d) features a conductivity ratio of one between the

290 fracture and matrix continua; i.e., 50% of the macroscopic flow is performed in the

291 fractures and 50% in the matrix. The advective-dispersive mixing between the fracture

292 and the matrix flow is so intense that the local concentrations equilibrate very fast,

293 despite the still significant velocity-difference ratio of 250 between the two media. We

294 present concentration contours at 20 days because the matrix blocks in Sectors 3 and 4

295 are completely contaminated after less than 100 days. (With a transport velocity of about

296 0.02 m/d in the matrix, a particle needs about 50 days to migrate along the two sectors, as

297 shown in Figure 3(d).) The breakthrough curves in Figure 4(d) resemble those of

298 advective-dispersive transport in a homogeneous medium; it seems that an almost

299 continuous front is moving through the formation.

300

301 **3   CTRW Modeling of the Fractured-Rock Transport Problem**

302 **3.1   Physical Motivation and Model Formulation**

303 The CTRW framework is a generalization of the classical Random Walk (RW) method

304 so often used in the hydrogeological literature to solve the advection-dispersion equation

305 (ADE) of a passive tracer in a porous domain. In the RW approach, tracer density is

306 obtained by following the evolution of an ensemble of random walkers taking

307 (uncorrelated) jumps of constant length at random (uniform) direction in the unit time.

308 CTRW generalizes this physical picture by allowing the walker to jump according to a

309 probabilistic distribution function (pdf), $\Psi(x,\tau)$, of the length of a jump, x, and the

310 retention time, τ, at a given location, while keeping a uniform random distribution for the

311 jump direction. Assuming that the probability of the length of the jumps and the retention

312 time probability are statistically independent, we write $\Psi(x,\tau) = p(x)\psi(\tau)$, where p(x) is

313 the probabilistic distribution of the particle jump lengths, and $\psi(\tau)$ is the retention times

314 pdf. A detailed analysis of this uncoupling assumption can be found in Berkowitz et al.

315 (2006]. When both the p(x) and $\psi(\tau)$ pdfs have finite first and second moments, (e.g.,

316 uniform, decaying exponential), the CTRW and RW physical pictures can be considered

317 to be equivalent. If, however, either of the two has infinite variance (e.g., Cauchy, power-

318 law) than the CTRW yields qualitatively different physical pictures, and the random

319 paths are referred to as Levy walks and Levy flights, for the cases of infinite variance of

320   $\psi(\tau)$ and p(x), respectively. By taking an ensemble average over all the possible

321   realizations of the unresolved heterogeneity, it is possible to map the set of small-scale,

322   unresolved heterogeneities onto a probabilistic distribution of retention times, $\psi(\tau)$, that

323   contains all the information necessary to describe transport in a given heterogeneous

324   media. The p(x) pdf is assumed to have finite variance; from a physical point of view,

325   this means that the tracer is allowed to take only relatively short jumps—consistent with

326   the geological picture we have of a fractured porous matrix.

327

328   A comprehensive discussion of the CTRW and its relation to other upscaling methods can be found in the

329   recent review by Berkowitz et al. (2006). We refer to this review for the theoretical development of the

330   CTRW, while details regarding the numerical implementation can be found in Cortis and Berkowitz

331   (2005). In this work, we use, as the starting point of our analysis, the CTRW partial differential equation

332   (PDE) for the transport of a passive tracer. In its nondimensional form, the CTRW PDE that governs the

333   spatio-temporal evolution of the density of a passive tracer, c(x,τ), is (Dentz et al., 2004):

334   $$u\tilde{c}(x,u) - c_0(x) = -\tilde{M}(u)\partial_x\left[\tilde{c}(x,u) - \alpha\partial_x\tilde{c}(x,u)\right] \qquad (1)$$

335

336   where the tilde indicates the Laplace transform (LT) $\tilde{f}(u) = L[f(\tau)] = \int_0^\infty f(\tau)\exp(-u\tau)d\tau$,

337   u is the Laplace variable, $c_0(x)$ is the initial condition, α is the local dispersivity, and

338   $\tilde{M}(u)$ is a memory function that takes into account the nature of the heterogeneity and is

339   related to the retention times pdf, $\psi(u)$, by $\tilde{M}(u) = u\dfrac{\tilde{\psi}(u)}{1 - \tilde{\psi}(u)}$. In Equation (1), length

340   and times have been made nondimensional, such that the nondimensional transport

341   velocity is equal to unity. Equation (1) represents the time convolution of the memory

342 function M(τ) with the classical advection-dispersion operator, and for this reason this

343 class of models is referred to as nonlocal in time. Equation (1) reduces to the classical

344 ADE when $\tilde{M}(u) = 1$; i.e., M(τ)=δ(τ), which implies an exponentially fast decay of the

345 retention times pdf, $\tilde{\psi}(u) = \dfrac{1}{1+u}$, i.e., ψ(τ)=exp($-\tau$). It can also be shown that fractional

346 derivative models are special cases of the general CTRW formulation (Berkowitz et al.,

347 2006).

348

349 The CTRW interpretation of the dispersivity α is different from the classical advection-

350 dispersion equation (ADE). In the ADE, α represents a typical characteristic length of the

351 small features of the systems, e.g., the pore-throat size. This interpretation has been a

352 problematic one from its inception, and has led to a vast literature on the so-called

353 macroscopic dispersion tensor, i.e., the attempt of explaining the scale-dependent

354 spreading of observed tracer BTCs by means of an evolving characteristic length. Instead,

355 in the CTRW approach, α is defined as the ratio

$$\alpha = \frac{1}{2} \frac{\int p(x)x^2 \, \mathrm{d}x}{\int p(x)x \, \mathrm{d}x} . \tag{2}$$

356

357

358 The ψ(τ) pdf completely describes, in a probabilistic sense, the entire range of

359 interactions that a solute molecule experiences in its interactions with the fluid flow field.

360 Heterogeneities in the flow field have a strong influence on the retention-time probability

361 of staying in a given place for a given interval of time, as is the case for high retention

362 times in stagnation zones (such as those in low-permeability matrix blocks) and short

363   retention times for fast flow paths (such as those in interconnected fractures). In other

364   words, the CTRW approach smoothes out the unresolved heterogeneities and maps them

365   onto the $\psi(\tau)$ retention times pdf. This mapping has the effect of representing the overall

366   effect of the heterogeneities through a time-memory convolution, which reflects the

367   history of interactions within the system.

368

369   As discussed in Dentz et al., (2004), an algebraically decaying $\psi(t) \sim \tau^{-1-\beta}$ can explain a

370   power-law like type of decay for the tail of a breakthrough curve. This type of long

371   tailing is illustrated in Figure 5, where we plotted the solution of the ADE equation for a

372   dimensionless velocity of v=1 and a dimensionless dispersivity α=0.005 (solid blue line),

373   and the CTRW solution corresponding to the $\tilde{\psi}(u) = \dfrac{1}{1+u^{\beta}}$, with β=0.8, and α=0.005

374   (solid red line). We recall that the ADE solution corresponds to $\tilde{\psi}(u) = \dfrac{1}{1+u}$. The long

375   tailing in the CTRW solution is caused by the convolution of the memory function with

376   the ADE transport operator (solid blue line). We note that the explicit solution of the

377   CTRW equation is more than just a simple convolution of the memory function

378    $\tilde{M}(u)$ with the solution for the ADE equation (see ,e.g., the Appendix B of Dentz et al.,

379   2004,). Depending on the specific shape of $\psi(\tau)$, the CTRW model can reproduce the fast

380   early-time arrivals as well as the long tailing typical of fractured systems, as illustrated in

381   Figure 5.

382

383   Typically, the CTRW PDE is solved by postulating a simple functional form for $\psi(\tau)$ and

384   then fitting its model parameters to the experimental data. A number of $\psi(\tau)$ models are

385   described in detail in Berkowitz et al. (2006). Despite the wide success in fitting many

386   laboratory and field datasets, however, such simple functional forms may not be general

387   enough to describe the entire range of transport modes encountered in hydrogeological

388   applications (Anwar et al., 2007). Following this approach, we have tried to fit the BTCs

389   in Figure 4 with all the functional forms described in Berkowitz et al. (2006), with no

390   success. Attempts to generalize these functional forms to conform to the shape of these

391   BTCs also failed. Thus, a more general and less restrictive method needs to be used in

392   this case. For this reason, in this work we apply a nonparametric inversion algorithm

393   (NPIA) first described in Cortis (2007).

394

395   The NPIA is aimed at recovering the numerical approximation of the whole spectrum of

396   retention times that govern transport directly from the experimental data, without

397   postulating *a priori* a functional form for $\psi(\tau)$. While the details of the NPIA can be

398   found in Cortis (2007), below we summarize the salient features of the method. In the

399   NPIA, the $\psi(\tau)$ is given through its numerical representation in the time-interval interest

400   depending on the evolution of the breakthrough. This representation is obtained through

401   the numerical inversion of the numerical approximation of $\tilde{\psi}(u)$, determined via a

402   nonlinear numerical inversion of the best fit of the CTRW PDE solution to the numerical

403   Laplace-transformed data. The method is robust enough to reproduce all the known

404   functional forms for $\psi(\tau)$, and yet flexible enough to represent more complex-looking

405   BTCs. One of the most notable results of the application of the nonparametric approach

406   to nonlocal methods is that any given unresolved heterogeneity can be represented by a

407   family of retention-time probability distributions, $\psi(\tau|\alpha)$ of parameter α, where α is the

408   local dispersivity. In other words, any given set of breakthrough curves taken at different

409   sections, and/or concentration profiles taken at different times, can be fit equally well by

410   different $\psi(\tau)$, conditional to some reasonable value of α. This means that the dispersivity

411   α cannot be considered either an intrinsic or a scale-dependent parameter of the system.

412   Importantly, as no *a priori* value of α can be given or estimated from any type of

413   macroscopic measurement, it must be interpreted only as an ancillary parameter of the

414   retention-time probability distribution $\psi(\tau)$, which fully describes the transport. These

415   considerations hold true not only for systems exhibiting anomalous transport, but also for

416   normal transport, i.e., for the classical ADE Gaussian type of transport (Cortis, 2007).

417

418   **3.3   Application of the CTRW Method**

419

420   The first step in applying the CTRW model to the BTCs (shown in Figure 4) is the

421   definition of characteristic (dimensional) transport velocity v' and dispersivity α' for the

422   different fracture-matrix systems studied in Section 2.

423

424   As discussed earlier, in our CTRW model, the interaction between the fractures and the

425   porous matrix is fully taken into account via the introduction of the memory function

426     $M(\tau)$ (hence the probabilistic distribution of retention times, $\psi(\tau)$), which is convoluted

427   with the classical ADE transport kernel, i.e., $v'\partial_x\left[c(x,t)-\alpha'\partial_x c(x,t)\right]$. We thus need to

428   define reasonable values for the relevant parameters v' and α' of the classical ADE that

429   represent the local dispersion inside the porous matrix and along single fractures, without

430   accounting for their interaction.

431

432   One logical approach is to define the characteristic transport velocity of the composite

433   system in Figure 2 using the total flux through the fracture-matrix column (to calculate

434   the Darcy velocity) and the total porosity of the fractured porous medium (to convert

435   from Darcy to transport velocity). In other words, we calculate the velocity v' that

436   represents a homogeneous column conducting the same total flux and has the same pore

437   space as the fracture-matrix systems studied in Cases 1 through 4. Note that both these

438   quantities—total flux and porosity—can generally be measured or estimated in field

439   situations. Similarly, the dispersivity α' can be chosen such that it represents only local

440   dispersive effects in fractures and matrix blocks, and not the effects stemming from the

441   fracture-matrix interaction. The exact value of α' is not important because, as discussed

442   above, the application of the nonparametric inversion algorithm implies that equally good

443   fits of the CTRW equations on the BTCs data can be obtained for different (reasonable)

444   values of the dispersivity (Cortis, 2007). In this work, we selected a value of $\alpha'=0.25$ m,

445   that, as we will see in the discussion below, represent the characteristic dispersivity of

446   Case 4. Such value of α' is considerably smaller than the typical macrodispersivity

447   estimates (Gelhar, 1993).

448

449   We define dimensionless parameters as follows. Length-based quantities such as

450   horizontal distance or dispersivity are normalized with the total length of the model

451   domain, L=50 m. The four BTC locations shown in Figure 4, at 2, 10, 30, and 90 sectors

452   (1, 5, 15, 45 m), thus correspond to nondimensional distances of $x=[0.02, 0.1, 0.3, 0.9]$.

453   Nondimensional dispersivity is $\alpha=0.005$. The characteristic transport velocity calculated

454 above is normalized to unity, and time in the breakthrough curves is normalized such that

455 a particle migrating with unit velocity would arrive at the end of the column, x=1, at

456 nondimensional time τ=1. We then select the BTC calculated at x=0.1 as the reference

457 BTC for the CTRW model: this will be our "data." In other words, the breakthrough

458 results from the discrete simulations for the cross section at 10 sectors (Figure 4)

459 represent the data set over which the nonparametric inversion algorithm is fitted to. The

460 NPIA yields the $\psi(\tau|\alpha)$ retention time pdf, conditional to the chosen value of α. The

461 $\psi(\tau|\alpha)$ is then used to predict the BTCs at x=0.02, x=0.3, and x=0.9. This procedure is

462 conducted for all parameter cases, by keeping the value of α unchanged.

463

464 We recall that Case 1 represents the one bounding case in which a very small flux is

465 allowed to flow in the porous matrix (low permeability). Cases 2, 3, and 4 have

466 increasing matrix-permeability values, with Case 4 the other bounding case, in which an

467 equal amount of flux is allowed in the fractures and the porous matrix.

468

469 The results of the fitting procedure to Cases 1 through 4 are reported in Figure 6. In the

470 left panels of Figure 6, we plotted as solid lines the simulated BTCs at the four sections

471 x=[0.02, 0.1, 0.3, 0.9] (as calculated by the discrete numerical procedure), together with

472 the best fits obtained by means of our NPIA applied to the CTRW model (circles). The

473 ADE model $\alpha = 0.005$ is also reported for reference (dashed lines). In the right panel of

474 Figure 6, we plotted, in double logarithmic units as a solid line, the best fit $\psi(\tau)$ obtained

475 with the NPIA on the BTC at x=0.1 and as a reference the exponential function exp(-τ),

476 which represents the ADE model limit.

477

478   As we can see from Figure (6), the ADE model does a good job at fitting the BTCs in

479   Case 4 (for x=0.1) and predicting the BTC at the other sections. This can be seen also

480   from the best fit $\psi(\tau)$ (solid line), which is very close to the decaying exponential $\exp(-\tau)$

481   (dashed line), i.e., the ADE limit. In other words, the observed "correct" BTC of the

482   fracture-matrix system can be represented without explicitly accounting for unresolved

483   heterogeneities. This is not too surprising, considering the strong mixing between fracture

484   and matrix flow (Figure 3) and the typical symmetrical shape of the breakthrough curve

485   (Figure 4). In this case, however, the CTRW model is slightly more precise than the ADE.

486   Notice that the good agreement between the "correct" BTC and the ADE solution also

487   supports the determination of the characteristic transport velocity of the composite

488   system.

489

490   As the total flux in the system predominantly flows in the fractures for the cases with

491   small matrix permeability (Cases 1 through 3), the ADE fails in predicting the BTCs,

492   whereas the CTRW model provides excellent fits (for x=0.1) and predictions (for

493   x=[0.02, 0.3, 0.9]). (For the section at x=0.02, the CTRW model provides a correct

494   prediction only up to the time at which the reference BTC used to derive the $\psi(\tau)$ pdf (in

495   our examples the BTC at x=0.1) differs significantly from zero. In other words, because

496   of the inherent numerical instability of the numerical Laplace inversion algorithms (i.e.,

497   the oscillating behavior), the numerical approximation of $\psi(\tau)$ is not accurate enough to

498   back-propagate the BTC for small enough times.) The CTRW approach is capable of

499   representing transport processes for a wide range of fractured porous formations, ranging

500   from mobile-immobile systems with mostly diffusive mixing (Figure 3(a) for Case 1) to

501   mobile-mobile systems with diffusive as well as advective-dispersive mixing (Figures

502   3(b) and 3(c) for Cases 2 and 3).

503

504   In each of these three cases, the best-fit $\psi(\tau)$ pdfs consistently deviate from the decaying

505   exponential, which indicates the presence of a wider spectrum of characteristic retention

506   times in the fracture-matrix system. We can observe the graph of the best-fit $\psi(\tau)$ (solid

507   line) crossing the graph of the decaying exponential (dashed line). Retention times larger

508   than exp(-τ) are indications of faster tracer arrivals, whereas smaller values indicate

509   slower tracer arrivals. This behavior can be understood by recalling the characteristics of

510   the fracture-matrix interaction as shown in Figure 3. We also note that the best-fit $\psi(\tau)$

511   converges, for long times, to a decaying exponential behavior, a clear indication of a

512   truncation time for the transport process (Dentz et al, 2004). Consistent with this

513   observation, the crossing time decreases with the increase of the matrix permeability.

514

515   It is also worth pointing out that the estimated $\psi(\tau)$ pdfs show a $\tau^{-1/2}$ slope for Cases 1

516   through 3, which is often observed in field conditions and interpreted as macroscopic

517   matrix diffusion. While Cases 1 and 2 are definitely diffusion dominated in the matrix,

518   Case 3 exhibits clearly the effect of advective transport through the matrix blocks. It

519   appears that diffusive and advective interaction between fractures and matrix lead to the

520   same slope in the estimated $\psi(\tau)$ pdfs. This suggests that the macroscopic values of

521   matrix diffusion determined in field conditions, which are often larger than those

522   observed in laboratory conditions, may include contributions stemming from advective

523   transport in the porous matrix. A interesting topic of research would be a study of the

524   relationship between the transition cut-off time from a $\tau^{-1/2}$ slope to a decaying

525   exponential behavior in the $\psi(\tau)$, and its dependence on the permeability characteristics

526   of the fractures and the matrix.

527

528   Note that the value for dispersivity α remains unchanged for the four cases, so that the

529   transport is completely defined by the $\psi(\tau|\alpha)$ pdf. Furthermore, within each individual

530   case, a single value of α is used to describe the BTCs for the four locations, whereas a

531   macrodispersivity approach would require a scale-dependent and much larger value of

532     $\alpha = \alpha(x)$. Our sensitivity study indicates that the quality of the CTRW fitting results does

533   not depend on the particular (small) value of α, in accordance with the results of Cortis

534   (2007) describing the existence of a family of residence time pdfs parameterized in α.

535   This confirms our initial conjecture that small values of α can be thought of as

536   accounting for the small local dispersion and diffusion phenomena happening in the

537   individual fractures and matrix blocks, whereas the fracture-matrix interaction can be

538   represented by a memory function related to the tracer retention-times probabilistic

539   distribution.

540

541

542

543   **4.   Conclusions**

544 We have presented a study of the tracer-transport interaction in a composite

545 hydrogeological system consisting of interconnected fractures and porous permeable

546 matrix blocks. Four sensitivity cases, covering a wide range of matrix permeability

547 values, exhibited a macroscopic transport behavior strongly dependent on the intrinsic

548 heterogeneity of the fractured rock (i.e., fractures versus matrix) and the characteristics of

549 local fracture-matrix interaction processes. Using results from numerical experiments

550 employing a discrete (microscopic) representation of fractures and matrix, we

551 investigated the possibility of the Continuous Time Random Walk (CTRW) framework

552 for predicting the observed macroscopic transport processes in such composite media.

553

554 Our results indicate that:

555   1. The CTRW offers a valid and robust alternative to classical approaches used for

556   fractured porous media (such as dual-continuum models), with a clear physical

557   interpretation and a parsimonious number of parameters;

558   2. The anomalous transport observed in the numerical experiments can be fully

559   characterized by the probabilistic distribution function (pdf) of retention times,

560        $\psi(\tau)$, which stochastically describes the full range of interactions between the

561   fractures and porous matrix;

562   3. The $\psi(\tau)$ pdf can be extracted by means of a nonparametric inversion algorithm

563   fitted on the observed breakthrough data at a given location, which fully

564   characterizes the transport at all other locations;

565   4. The characteristic transport velocity used in the CTRW approach can be

566   calculated from the total composite flux and the total composite porosity of the

567   fractured formation;

568   5. The dispersivity α used in the CTRW is not scale-dependent, such that one value

569   of α can be used for all sensitivity cases and locations. Moreover, the relatively

570   small value used for α represents the local dispersion in single fractures or matrix

571   blocks, but does not need to account for the complex interaction between fractures

572   and matrix that leads to the anomalous macroscopic behavior. As discussed

573   above, the latter is fully characterized by the pdf of retention times;

574   6. Anomalous early-time arrivals can also be represented in the CTRW framework,

575   and are characterized by values of $\psi(\tau) > \exp(-\tau)$ for times smaller than some

576   crossover value τ', whereas the slow late-time arrivals are characterized by values

577   of $\psi(\tau) < \exp(-\tau)$.

578

579   Future work will focus on CTRW applications to more disordered fracture-matrix

580   systems, looking at the effects of random fracture structures or evaluating the impact of

581   microscopic heterogeneities within the fractures or the porous matrix, hence requiring a

582   local $\psi(\tau)$ for these local structures. We will also attempt to apply the CTRW methods

583   developed here to field data from fractured porous media.

584

585

586

Acknowledgments

References

Ahmadi, A., Quintard, M., Whitaker, S. (1998), Transport in Chemically and Mechanically Heterogeneous Porous Media V. Two-Equation Model for Solute Transport with Adsorption, Advances in Water Resources, 22(1), pp. 59-86.

Anwar, S., Cortis, A., and Sukop, M.C. (2007) Lattice Boltzmann Simulation of Solute Transport in Heterogeneous Porous Media with Conduits to Estimate Macroscopic Continuous Time Random Walk Model Parameters. Progress in Computational Fluid Dynamics(in press).

Barenblatt, G.E., Zheltov, I.P., Kochina, I.N. (1960), Basic Concept on the Theory of Homogeneous Liquids in Fissured Rocks, J. Appl. Math. Mech., Engl. Transl., 20, pp. 852-864.

Berkowitz, B., Bear, J., Braester, C. (1988), Continuum Models for Contaminant Transport in Fractured Porous Formations", Water Resources Research, 24(8), pp. 1225-1236.

Berkowitz, B. (2002), Characterizing Flow and Transport in Fractured Geological Media: A Review, Advances in Water Resources, 25, pp. 861-884.

Berkowitz, B., Cortis, A., Dentz, M., Scher, H. (2006), Modeling Non-Fickian Transport in Geological Formations Rev. Geophys., Reviews of Geophysics, 44 (2): Art. No. RG2003

Bibby, R. (1981), Mass Transport of Solutes in Dual-Porosity Media, Water Resources Research, 17(4), pp. 1075-1081.

612   Birkholzer, J., Rubin, H., Daniels, H., Rouve, G. (1993a): Contaminant Advection and

613   Spreading in a Fractured Permeable Formation: Part 1. Parametric Evaluation and

614   Analytical Solution, Journal of Hydrology, 144, pp. 1-33.

615   Birkholzer, J., Rubin, H., Daniels, H., Rouve, G. (1993b): Contaminant Advection and

616   Spreading in a Fractured Permeable Formation: Part 2. Numerical Simulation, Journal

617   of Hydrology, 144, pp. 35-58.

618   Birkholzer, J., Rouve, G. (1994): Dual-Continuum Modeling of Contaminant Transport

619   in Fractured Formations, Proceedings X International Conference on Computational

620   Methods in Water Resources, Heidelberg, Germany.

621   Boano, F., Packman, A.I., Cortis, A. Revelli, R., Ridolfi, L. (2007), A continuous time

622   random walk approach to the stream transport of solutes, Water Resources Research,

623   doi:10.1029/2007WR006062, in press.

624   Bijeljic, B., Blunt, M. (2006), Pore-scale modeling and continuous time random walk

625   analysis of dispersion in porous media, Water Resources Research, Vol. 42(1): 5. doi:

626   10.1029/2005WR004578. issn: 0043-1397.

627   Bodin, J., Delay, F., de Marsily, G. (2004), Solute transport in a single fracture with

628   negligible matrix permeability. 2. Mathematical formalism, Hydrogeology Journal

629   Vol. 11, pp. 434-454.

630   Cherblanc, F., Ahmadi, A., Quintard, M. (2003), Two-Domain description of Dispersion

631   in Heterogeneous Porous Media: Calculation of Macroscopic Properties, Water

632   Resources Research, 39(6), pp. 1154ff.

633   Cherblanc, F., Ahmadi, A., Quintard, M. (2007), Two-Domain Description of Solute

634   Transport in Heterogeneous Porous Media: Comparison Between Theoretical

635   Predictions and Numerical Experiments, Advances in Water Resources, 30, pp. 1127-

636   1143.

637   Cortis, A. (2007), Péclet-dependent memory kernels for transport in heterogeneous media,

638   Phys. Rev. E 76, 030102(R).

639   Cortis, A. and Ghezzehei T.A. (2007), On the transport of emulsions in porous media, J.

640   Colloid and Interface Science 313 (1): 1-4.

641   Cortis, A. and Knudby C. (2006), A CTRW approach To Anomalous Transient Flow in

642   Heterogeneous Porous Media, Water Resour. Res., 42 (10): Art. No. W10201.

643   Cortis, A., Harter, T., Hou, L., Atwill, E. R., Packman, A., Green, P. (2006), Long-time

644   Elution of Cryptosporidium Parvum Oocysts in Porous Media Water Resour. Res., 42

645   (12): Art. No. W12S13.

646   Cortis A. and Berkowitz B. (2005), Computing ''Anomalous'' Contaminant Transport in

647   Porous Media: The CTRW MATLAB Toolbox, Ground Water Vol. 43, No. 6,

648   November–December 2005, 947–950.

649   Cortis, A., Chen, Y., Scher, H., Berkowitz, B. (2004), Quantitative characterization of

650   porescale disorder on transport in "homogeneous" granular media. Phys. Rev. E,

651   70(4):041108.

652   Cortis, A. and Berkowitz, B. (2004), Anomalous transport in "classical" soil and sand

653   columns, Soil Sci. Soc. Am. J., 68: 1539-1548.

654   Dentz, M., Berkowitz, B. (2003), Transport Behavior of a Passive Solute in Continuous

655   Time Random Walks and Multirate Mass Transfer, Water Resources Research, 39(5),

656   pp. 1111ff.

657   Dentz, M., Cortis, A., Scher, H., and Berkowitz, B. (2004). Time behavior of solute

658   transport in heterogeneous media: transition from anomalous to normal transport.

659   Adv. Water Resour., 27(2):155–173, doi:10.1016/j.advwatres.2003.11.002

660   Dykhuizen, R.C. (1990), A New Coupling Term for Dual-Porosity Models, Water

661   Resources Research, Vol. 26, No. 2, pp. 351-356.

662   Feehley, C.E., Zheng, C., Molz, F.J. (2000), A Dual-Domain Mass transfer Approach for

663   Modeling Solute Transport in Heterogeneous Aquifers: Application to the

664   Macrodispersion Experiment (MADE) Site, Water Resources Research, 36(9), pp.

665   2501-2515.

666   Flach, G.P., Crisman, S.A., Molz, F.J. (2004), Comparison Between Single-Domain and

667   Dual-Domain Subsurface Transport Models, Groundwater, 42(6), pp. 815-828.

668   Gerke, H.H., van Genuchten, M.T. (1993a), A Dual-Porosity Model for Simulating the

669   Preferential Movement of Water and Solutes in Structured Porous Media, Water

670   Resources Research, 29(2), 305-319.

671   Gerke, H.H., van Genuchten, M.T. (1993b), Evaluation of a First-Order Water Transfer

672   Term for Variably Saturated Dual-Porosity Flow Models, Water Resources Research,

673   Vol. 29(4), pp. 1225-1238.

674   Gwo, J-P., O'Brien, R., Jardine, P.M. (1998), Mass Transfer in Structured Porous Media:

675   Embedding Mesoscale Structure and Microscale Hydrodynamics in a Two-Region

676   Model, Journal of Hydrology, 208, pp. 204-222.

677   Haggerty, R., Gorelick, S.M. (1995), Multiple-Rate Mass Transfer for Modeling

678   Diffusion and Surface reactions in Media with Pore-Scale Heterogeneity, Water

679   Resources Research, 31(10), pp. 2383-2400.

680   Huyakorn, P.S., Lester, B.H., Faust, C.R. (1983a), Finite Element Techniques for

681   Modeling Groundwater Flow in Fractured Aquifers, Water Resources Research, 19(4),

682   pp. 1019-1035.

683   Huyakorn, P.S., Lester, B.H., Mercer, J.W. (1983b), An Efficient Finite Element

684   Technique for Modeling Transport in Fractured Porous Media: 1. Single Species

685   Transport, Water Resources Research, Vol. 19(3), pp. 841-854.

686   Huyakorn, P.S., Lester, B.H., Mercer, J.W. (1983c), An Efficient Finite Element

687   Technique for Modeling Transport in Fractured Porous Media: 2. Nuclide Decay

688   Chain Transport, Water Resources Research, Vol. 19(5), pp. 1286-1296.

689   Lagendijk, V.R. (2005), Stofftransportvorgänge in Festgesteinsaquiferen: Analyse von

690   Tracerdurchbruchskurven zur Identifikation eines geeigneten Mehrkontinuum-

691   Ansatzes, Ph.-D. Thesis, Proceedings 140, IWW, Aachen University of Technology.

692   Landereau P., Noetinger B., Quintard M., (2001), Quasi steady two equation models for

693   transport in fractured porous media: Large scale properties for densely fractured

694   systems, Advances in Water Resources, Vol. 24(8), pp. 863-876.

695   Neuman, S.P. (2005), Trends, Prospects and Challenges in Quantifying Flow and

696   Transport Through Fractured Rocks, Hydrogeology Journal, 13, 124-147.

697   Noetinger B., Estebenet T., and Landereau P., (2001), A direct determination of the

698   transient exchange term of fractured media using a continuous time random walk

699   method, Transport in Porous Media, Vol. 44, pp. 539-557.

700   Noetinger B., Estebenet T., and Quintard M., (2001), Up scaling flow in fractured media:

701   equivalence between the large scale averaging theory and the continuous time random

702   walk method, Transport in Porous Media, Vol. 43, pp. 581-596.

703   Roth, K., Jury, W.A. (1993): Linear Transport Models for Adsorbing Solutes, Water

704   Resources Research, Vol. 29(4), pp. 1195-1204.

705   Rubin, H., Soliman, A.M., Birkholzer, J., Rouve, G. (1996): Transport of a Tracer Slug in

706   a Fractured Permeable Formation, Journal of Hydrology, 176, pp. 153-180.

707   Simunek J., Jarvis, N.J., Van Genuchten, M.T., Gaerdenaes, A. (2003), Review and

708   Comparison of Models for describing Non-Equilibrium and Preferential Flow and

709   Transport in the Vadose Zone, Journal of Hydrology, 272, pp. 14-35.

710   Teutsch, G. (1990), An Extended Double-Porosity Concept as a Practical Modeling

711   Approach for Karstified Terranes, Int. Symp. Field Seminar on Hydrogeological

712   Processes in Karst Terranes, 7. - 17. Oct. 1990, Antalya, Turkey.

713   Zimmerman, R.W., Chen, G., Hadgu, T., Bodvarsson, G.S. (1993), A Numerical Dual-

714   Porosity Model with Semianalytical Treatment of Fracture/Matrix Flow, Water

715   Resources Research, Vol. 29(7), pp. 2127-2137.

716   Zimmerman, R.W., Bodvarsson, G.S., Kwicklis, E.M. (1990), Adsorption of Water into

717   Porous Blocks of Various Shapes and Sizes, Water Resources Research, Vol. 26(11), pp.

718   2797-2806.

719   Table 1: Geometry and properties chosen for discrete simulation

Parameter	Value	Unit
Fractures		
Fracture Spacing, B	0.707	m
Angle Between Fractures and x – Direction, θ	45	°
Aperture, a	10^{-4}	m
Hydraulic Conductivity of Single Fracture[1]**,** K_s^F	703	m/d
Continuum Conductivity in x – Direction[2]**,** K^F	9.94×10^{-2}	m/d
Equivalent Continuum Porosity[3]**,** n^F	2.83×10^{-4}	-
Longitudinal Dispersivity Along Single Fracture, α_l^F	0.01	m
Effective Diffusion in Single Fracture Coefficient, D_{mo}^F	10^{-4}	m²/d
Matrix[4]		
Porosity, n^M	0.05	-
Hydraulic Conductivity, K^M	case dependent	m/d
Longitudinal Dispersivity, α_l^M	0.01	m
Transverse Dispersivity, α_t^M	0.001	m
Effective Diffusion Coefficient[5]**,** D_{mo}^M	2.0×10^{-5}	m²/d
Size of Matrix Blocks, $B \times B$	0.707×0.707	m²
Other		
Hydraulic Gradient in x - Direction, J	0.01	-
Sector Length, L	0.5	m

720   [1] Calculated from parallel plate assumption as follows: $K_s^F = g(2b)^2 / 12\nu$

721   [2] Calculated from geometry considerations as follows: $K^F = K_s^F \cos\theta /(B\sin\theta)$

722   [3] Calculated from geometry considerations as follows: $n^F = a /(B \sin\theta \cos\theta)$

723   [4] Properties are given for unit bulk volume of the rock matrix

724   [5] Includes effect of tortuosity, assumed to be 0.2

725

726

726   Table 2:   Sensitivity Cases

	Case 1	**Case 2**	**Case 3**	**Case 4**
Formation Type	e.g., crystalline rock, shale	e.g., porous sandstone, limestone		
Matrix Hydraulic Conductivity	8.3×10^{-6} m/d	2×10^{-3} m/d	8.3×10^{-3} m/d	9.94×10^{-2} m/d
Ratio Fracture to Matrix Continuum Conductivity	$\approx 12{,}000$	50	12	1
Ratio Fracture to Matrix Transport Velocity[1]	$\approx 3 \times 10^{6}$ m/d	$\approx 12{,}400$	$\approx 3{,}000$	250
Type of Fracture-Matrix Interaction[2]	Almost Purely Diffusive	Mostly Diffusion	Diffusion and Advection	Mostly Advection, Strong Mixing
Breakthrough Characteristics[2]	Rapid Response, Long Tail	Between Cases 1 and 4		Typical ADE[3] without tailing

727   [1] Fracture transport velocity is measured along fracture axis.

728   [2] Based on Birkholzer & Rouve (1994)

729   [3] ADE: Advection-Dispersion Equation

730

731
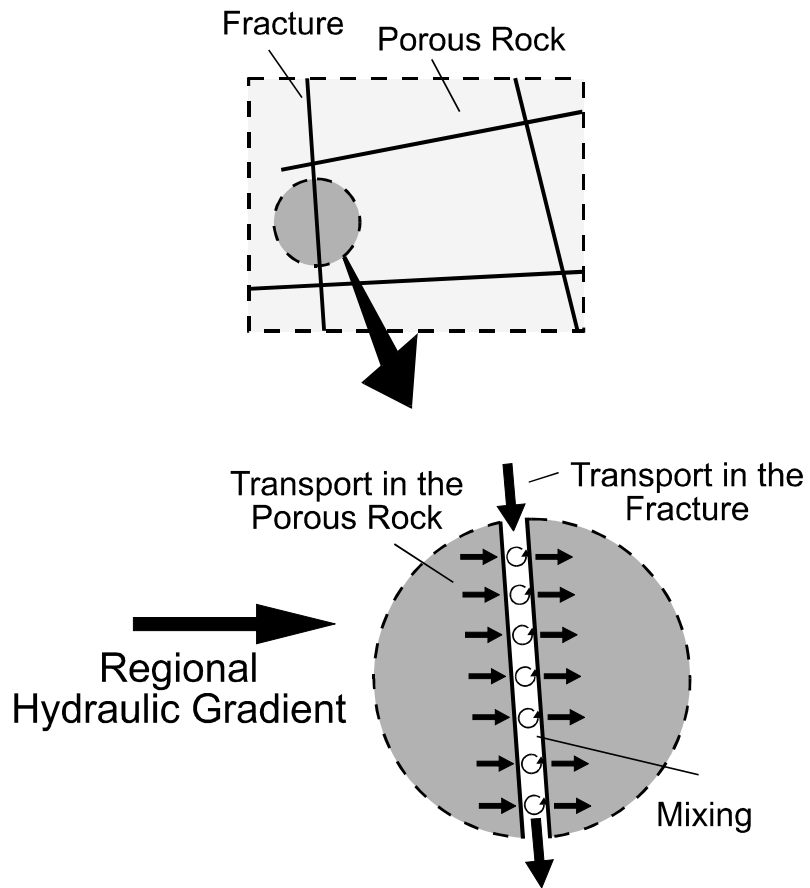
731

732

733   Figure 1: Schematic showing the mixing between fracture and matrix flow as a result of

734   convective transport in the matrix

735

736
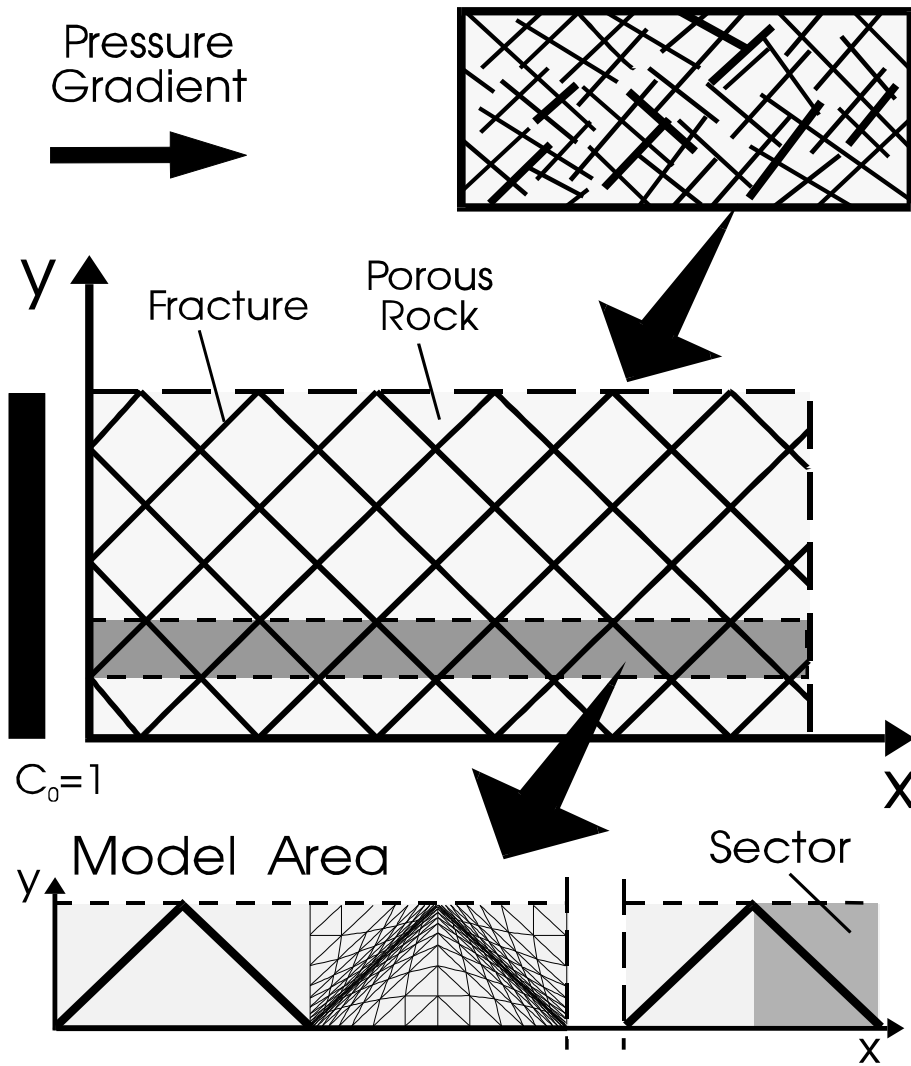
736

737   Figure 2.   Discrete representation in idealized fracture network. Flow and transport is

738   from left to right, with a concentration boundary condition on the left side. The total

739   domain is 100 sectors long.

740

741
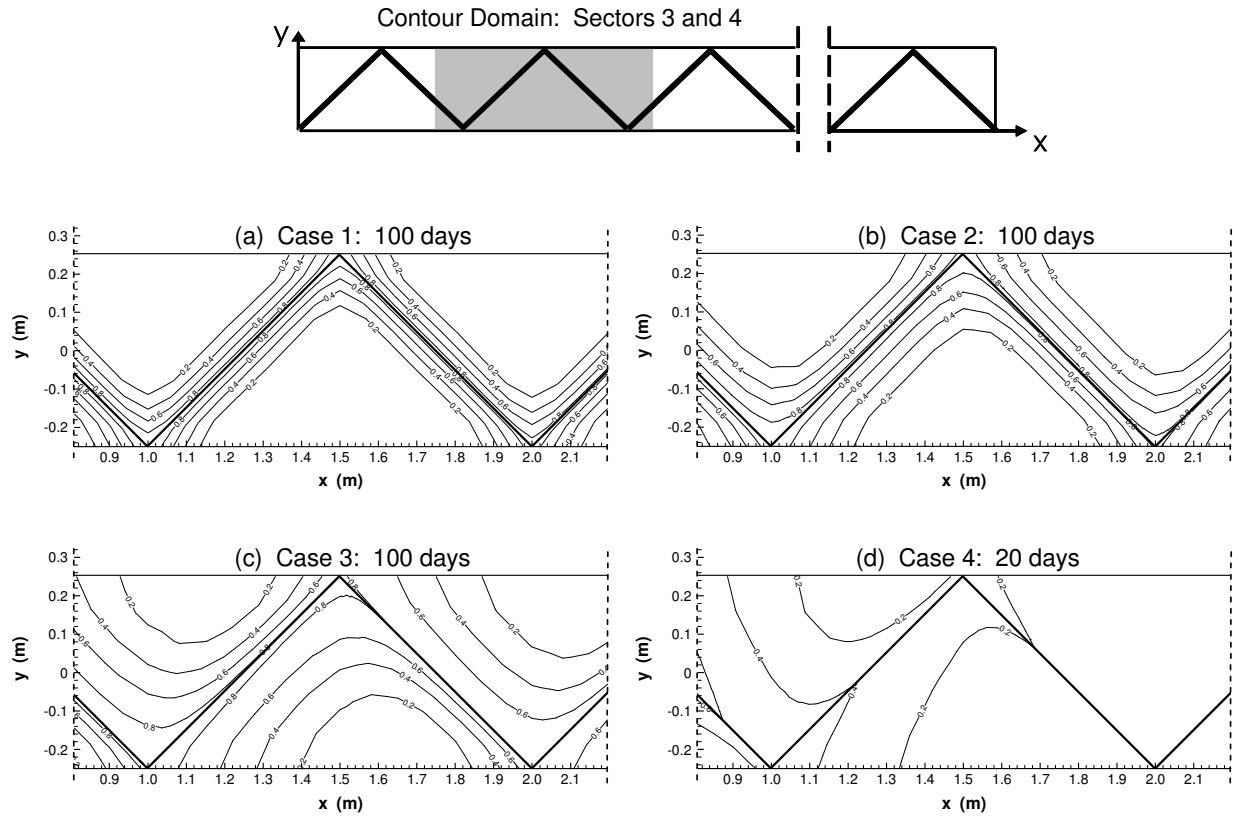
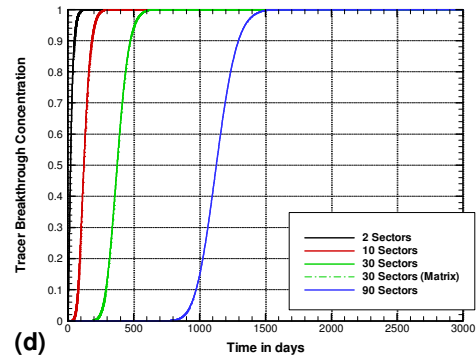Figure 3.   Matrix concentrations from discrete simulations displayed in sectors 3 and 4 of the model domain.

744

(a)

745

(b)

(c)

(d)
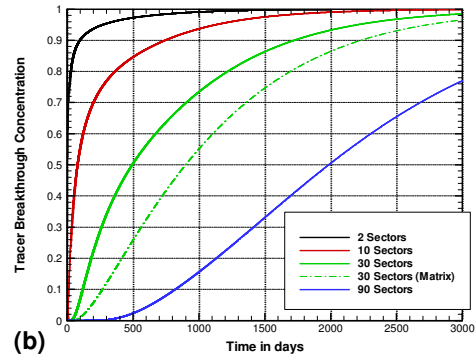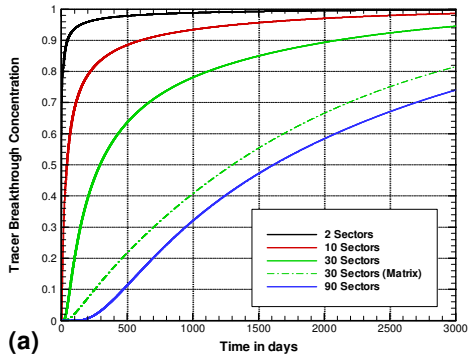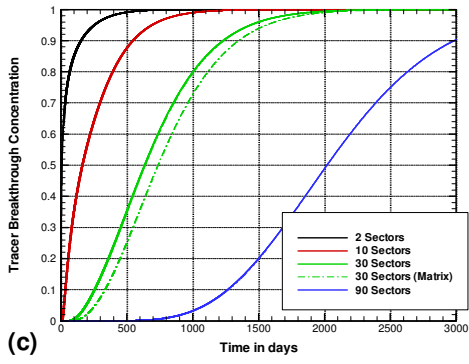
746   Figure 4.   Breakthrough curves for (a) Case 1, (b) Case 2, (c) Case 3, and (d) Case 4,

747   measured at different locations along the model domain.

748

748
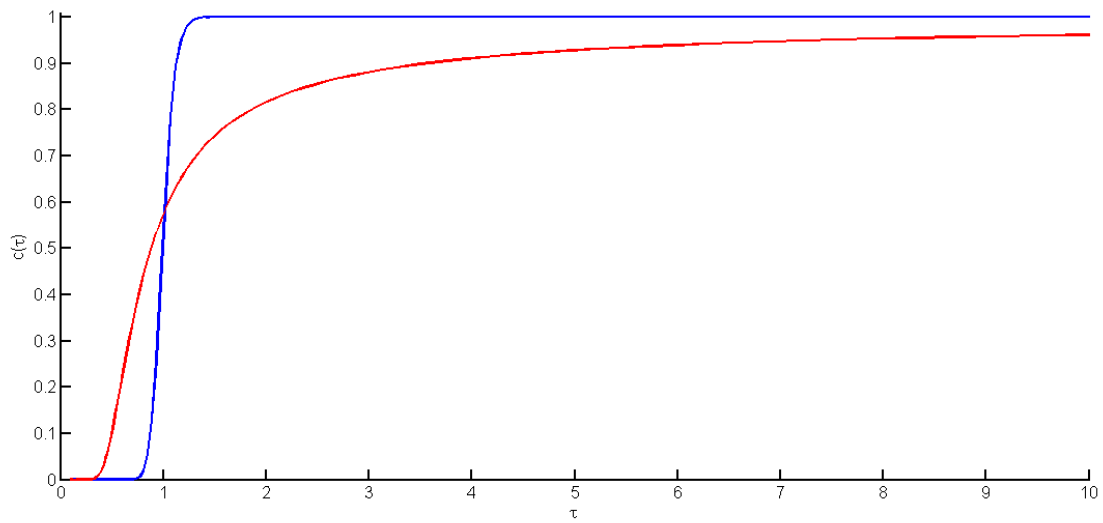
Figure 5. ADE solution (solid blue line) and CTRW solution (solid red line), for the

same value of the non-dimensional dispersivity α=0.005. For the CTRW

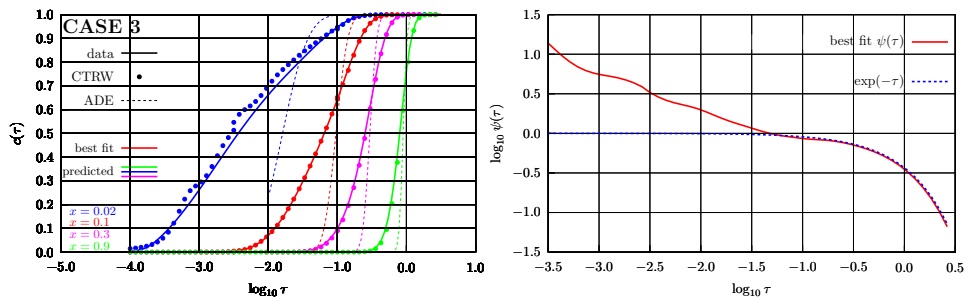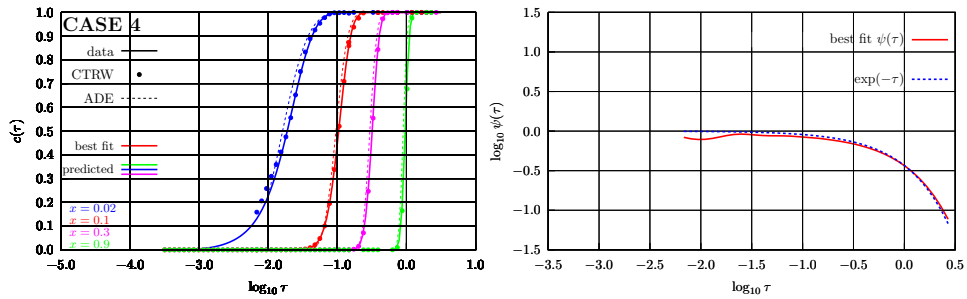solution, $\tilde{\psi}(u) = \dfrac{1}{1+u^{\beta}}$, with β=0.8.

752

753

753

754

755

756

757
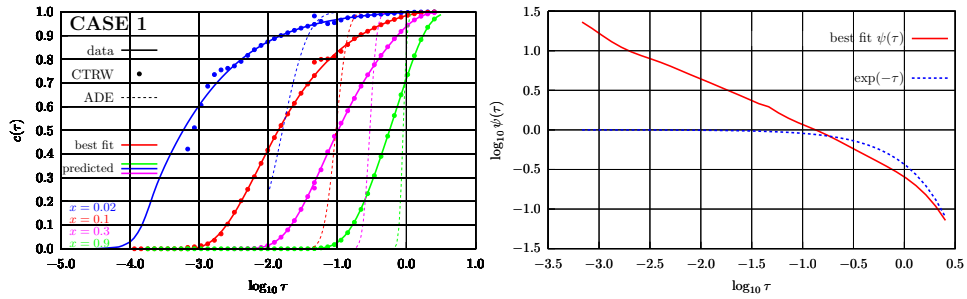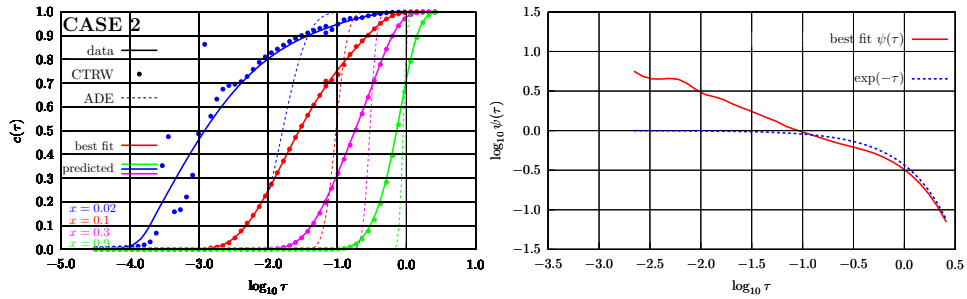
Figure 6: Best fit results of the CTRW model. Cases 1-4, (top to bottom) represent systems with increasing values of the porous matrix (See Table 2). In the left panel we compare the discrete numerical computations (solid lines), with the CTRW model (circles) and the ADE model (dashed lines). The breakthrough curves are calculated at four different sections, x=0.02, 0.1, 0.3, and 0.9. In the right panel, we plot the best fit probabilistic distribution of retention times, $\psi(\tau)$ (solid lines), and for comparison the decaying exponential $\exp(-\tau)$ (dashed lines), the classical ADE limit.